Mostafa Agour ; Claas Falldorf ; Fatima Taleb ; Enrique Castro-Camus ; Martin Koch ; Ralf B. Bergmann

Shear interferometry for terahertz wavefront sensing

Conference paper as: published version (Version of Record)

DOI of this document*(secondary publication): https://doi.org/10.26092/elib/3814

Publication date of this document: 16/04/2025

* for better findability or for reliable citation

Recommended Citation (primary publication/Version of Record) incl. DOI:

Mostafa Agour, Claas Falldorf, Fatima Taleb, Enrique Castro-Camus, Martin Koch, and Ralf B. Bergmann "Shear interferometry for terahertz wavefront sensing", Proc. SPIE 12134, Terahertz Photonics II, 121340B (31 May 2022); https://doi.org/10.1117/12.2621696

Shear-interferometry for terahertz wavefront sensing

Mostafa Agour[a,b], Claas Falldorf[a], Fatima Taleb[c], Enrique Castro-Camus[c,d], Martin Koch[c], and Ralf B. Bergmann[a,e]

[a]BIAS-Bremer Institut für angewandte Strahltechnik, 28359 Bremen, Germany
[b]Aswan University, Faculty of Science, Department of physics, 81528 Aswan, Egypt
[c]Faculty of Physics and Material Sciences Center, Philipps-Universität Marburg, Renthof 5, 35032 Marburg, Germany
[d]Centro de Investigaciones en Optica, A.C., Loma del Bosque 115, Lomas del Campestre, Leon, Guanajuto 37150, Mexico
[e]University of Bremen, MAPEX Center for Materials and Processes and Faculty of Physics and Electrical Engineering, 28359 Bremen, Germany

ABSTRACT

We propose a new solution for sensing a terahertz (THz) wavefront based on a THz reference-less shear interferometer. The key component of the experimental configuration of the proposed interferometer is a THz Ronchi phase grating (RPG). The RPG is custom designed and fabricated for a 0.28 THz source using mechanical milling on a block of high-density polyethylene (HDPE) with a computer numerical control (CNC) machine. It acts as a shearing element that generates two diffraction orders, thereby creating two laterally shifted copies of the investigated wavefront in the sensor plane where a THz camera is placed. The direction of the shear can be varied by rotating the grating. Since the grating is a phase grating, the diffraction efficiency is very high. The approach is verified experimentally by demonstrating interferograms of a spherical wave and wavefront reconstruction from five different shears using a gradient-based iterative process.

Keywords: Terahertz wavefront, shear-interferometry, phase grating, wavefront sensing, phase measurements

1. INTRODUCTION

The use of terahertz (THz) radiation has attracted the attention of a broad set of researchers because it has interesting properties compared to other spectral bands.[1,2] For instance, THz-waves are non-ionizing and thus harmless for biological tissues and humans, unlike x-rays. For this reason predominantly sensing[3,4] and imaging[5–7] applications are discussed. In addition, THz-waves penetrate a wide range of material packages which are optically opaque in contrast to the visible band. These properties broaden the field of applications to include non-destructive testing to inspect agricultural products and food,[8–10] medical imaging,[11–13] and communication.[14–19] In turn, this stimulates the development of new core techniques providing novel THz-components, including sources and detectors.

Sensing both, the amplitude and also the phase of THz radiation, as it was achieved by THz digital holography (DH), plays an important role to improve the applicability of THz in many areas, such as quality control[20] and biology.[21] Sensing a THz beam has been achieved by using full-field single beam methods such as in-line holography, iterative and deterministic multiple plane phase retrieval (PR)[22–24] and ptychography.[25] However, these techniques require additional information such as recording holograms or intensity patterns of the diffracted wave field across different planes, in analogy to the implementation in the visible band, which is required to solve the associated reconstruction inverse problem.[26–29] As an example, in-line THz DH suffers from the overlapping of the zero-order and twin-image artifacts reducing the resolution of the reconstruction. One way to overcome this problem is capturing multiple in-line holograms across different axial planes. Thus, in in-line DH, PR and ptychography the recording process is time consuming and is highly sensitive to mechanical vibration.

Further author information: (Send correspondence to Mostafa Agour)
Mostafa Agour: E-mail: agour@bias.de, Telephone: +49 (0)421 21858015

Terahertz Photonics II, edited by Mona Jarrahi, Sascha Preu, Dmitry Turchinovich, Proc. of SPIE Vol. 12134, 121340B · © 2022 SPIE · 0277-786X · doi: 10.1117/12.2621696

Moreover, the reconstruction process for, both PR and ptychography, is based on the presence of diversity of the captured intensity patterns. Consequentially, smooth wavefronts, such as plane waves, can not be analyzed. Additionally, off-axis THz-DH, requires a reference wave with known characteristics and both temporally and spatially coherent illumination since it is based on the interference of diffracted light with a reference wave. This constitutes considerable drawbacks, because the characterization of an a-priori unknown THz wave emitted by an antenna or self-luminous object, is cumbersome.

Here, we propose a solution to these dilemmas based on a THz referenceless shear interferometer. This is achieved in a simple setup by placing a THz Ronchi phase grating (RPG) between the THz source and the camera sensor. The RPG[30] acts as a shearing element that generates two diffraction orders, thereby creating two laterally shifted images in the sensor plane. The direction of the shear can be varied by rotating the grating. Since the RPG is a phase grating, the diffraction efficiency is very high, approx. 80% of the diffracted light is diffracted to the ± 1 orders. The approach is verified experimentally by demonstrating interferograms of spherical waves. For this purpose, five different shear measurements are acquired. With them, the wavefront reconstruction is achieved using a gradient-based iterative process.

2. CONCEPT OF THE THZ SHEAR INTERFEROMETER

Figure 1 shows a scheme of a simple common-path shear interferometer. It consists of three main components; a continuous wave (CW) THz-source, a Ronchi phase grating (RPG) which represents the shear element and a linear THz camera sensor. The distance between the source and the RPG is z_1, while z_2 is the distance between the RPG and the camera. Such a simple setup is used here for measuring THz spherical wavefronts. Lets assume that the emitter is a point source which generates a spherical wave with U_1 being the spherical wave field directly in the front of the RPG. Thereafter, U_1 is modulated by the transmittance G of the RPG and a modified wave field U_2 is generated directly behind the RPG. Such a modified wave field then propagates to generate a new wave field $U = \mathcal{P}\{U_2\}$ at the camera plane, where $\mathcal{P}$ is a propagation operator used to propagate the modulated wave field to the camera plane.

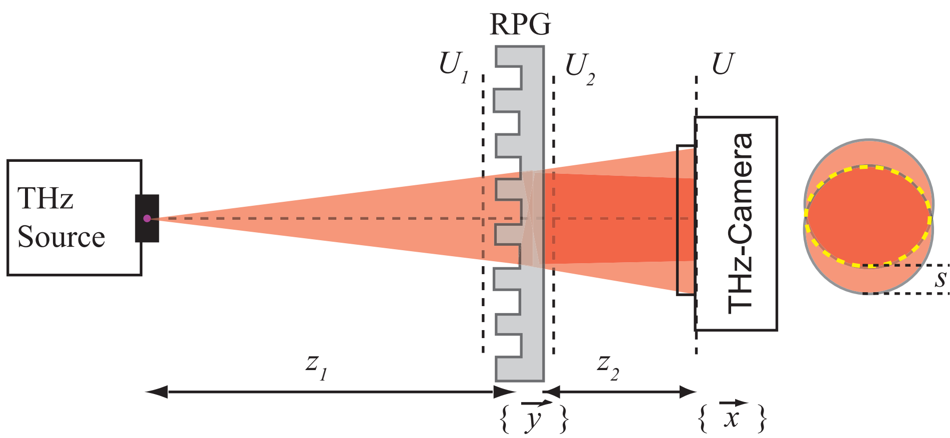

Figure 1. Schematic of the experimental configuration used to measure the THz wavefronts. U_1 and U_2 are the complex amplitude of the wave field before and after transmitted through the a Ronchi phase grating (RPG) inserted in the plane $\{\vec{y}\}$ which is z_1 away from the THz source. U is the wave field generated across the output plane $\{\vec{x}\}$ where a THz camera sensor is used to capture the interference pattern generated from the overlap between the ± 1 diffraction orders of the RPG. At a distance of z_2 the two ± 1 diffraction orders are separated by s which refers to as the shear.

Figure 2 shows a scheme of the grating for illustration purposes. Since the RPG is the key component of the setup, we discuss its properties here in more detail. Lets assume a RPG with a clear aperture of D and grating period of a. For a grating vector $\vec{g}$ defined as

$$\vec{g} = \frac{1}{a} \begin{pmatrix} \sin \alpha \\ \cos \alpha \end{pmatrix} , \tag{1}$$

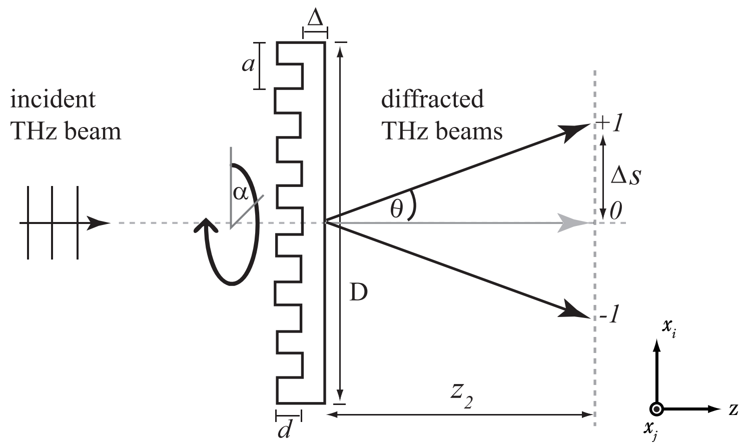

Figure 2. Schematic representation of the THz beam diffraction by a phase Ronchi grating. The Ronchi grating has a clear aperture of a diameter (D), and a thickness of (Δ), a grating period of a, a depth (height of the groves) of d. The $+1$, 0 and -1 refer to the diffraction orders of the grating, θ represents the diffraction angle, Δs represents the half of the shear s and α is the rotation angle used to change the direction of the shear. For ideal depth d for a given wavelength the Phase Ronchi grating diffracts no intensity into the 0 order.

and depends on the grating orientation α and the period a, the grating modulations for the $+1$ and -1 diffraction orders can be given as $G_{+1} = \exp(\mathrm{i}2\pi\vec{g}\vec{x})$ and $G_{-1} = \exp(-\mathrm{i}2\pi\vec{g}\vec{x})$. Accordingly, the wave field U_c generated from the coherent superposition of the $+1$ and -1 diffraction orders can be written as

$$U_c(\vec{x}) = U_{+1}(\vec{x}) + U_{-1}(\vec{x}) = U(\vec{x}) \cdot \exp\left(\mathrm{i}2\pi\vec{g}\vec{x}\right) + U(\vec{x}) \cdot \exp\left(-\mathrm{i}2\pi\vec{g}\vec{x}\right) . \tag{2}$$

Thus, light diffracted to the two orders is modified with different linear phase ramps. Because we aim to fabricate an optimal RPG, the phase modulation introduced to the beam passing through it is important. Such a phase modulation is introduced by the periodically varying depth d of the grating which leads to a phase difference ϕ of

$$\phi = \frac{2\pi}{\lambda}(n-1)d\,, \tag{3}$$

where λ is the wavelength of the THz beam, n is the refractive index of the grating material and d is the depth of the grooves at the grating. Reducing the diffraction efficiency of the 0 and the even diffraction orders to zero requires that the phase difference $\phi = \pi$. Substituting this condition in Eq. (3) yields the ideal depth of the grating grooves to

$$d = \frac{\lambda}{2(n-1)}\,. \tag{4}$$

Such a grating structure will lead to a diffraction angle θ of

$$\theta = \sin^{-1}\left(\frac{\lambda}{a}\right)\,, \tag{5}$$

for the $+1$ and -1 diffraction orders respectively, assuming normal incidence to the grating surface. This angle causes the shift Δs of the $+1$ diffraction order at a distance of z_2 from the optical axis which can be calculated as

$$\Delta s = \frac{\lambda z_2}{a}\,, \tag{6}$$

where the distance z_2 is the distance between the grating and the camera sensor and assuming $z_2 >> s$. Accordingly, we can obtain the shear $s = 2\Delta s$ between the $+1$ and -1 diffraction orders. Thus, the wave field modulation by the RPG produces two mutually shifted copies of the wave field. Across the overlap zone between these two copies, as shown in Fig. 1, an interference pattern across the camera plane is generated. As an application, the characterization of the THz beam across the camera plane by measuring the amplitude and the wavefront will be discussed. For a spherical wave field propagating thought the setup, the spherical wave generated at the camera plane U_s can be written according to the Fresnel approximation as

$$U_s(\vec{x}) = \frac{A(\vec{x})}{z} \cdot \exp\left[\mathrm{i}kz\left(1 + \frac{|\vec{x}|^2}{2z^2}\right)\right]. \tag{7}$$

Where, $A(\vec{x})$ is the real amplitude of the spherical wave, $k = 2\pi/\lambda$ denotes the wavenumber and $z = z_1 + z_2$ is the distance between the THz source and the camera which in turn gives the beam radius of curvature. It is noted as a special case that the linear ramp modulation at the camera plane given in Eq. (2) leads to a shift of the test spherical wavefront. Accordingly, the intensity $I(\vec{x})$ of the interference pattern may be written as

$$\begin{aligned} I(\vec{x}) = |U_c(\vec{x})|^2 &= \left|U_s\left(\vec{x} - \frac{\vec{s}}{2}\right) + U_s\left(\vec{x} + \frac{\vec{s}}{2}\right)\right|^2 \\ &= I_0(\vec{x}) + 2\mathcal{R}\left\{U_s^*\left(\vec{x} - \frac{\vec{s}}{2}\right)U_s\left(\vec{x} + \frac{\vec{s}}{2}\right)\right\}, \end{aligned} \tag{8}$$

here, $I_0(\vec{x}) = 2|A(\vec{x})|^2/z^2$ is the background intensity assuming equal amplitudes of the two copies of the test wave field, $\mathcal{R}\{\cdots\}$ refers to as the real part of a complex number and $*$ refers to the complex conjugate. Notice, that $\mathcal{R}\{\cdots\}$ represents the interference terms which contain the phase information. Substituting Eq. (7) into Eq. (8), the interference term takes the form

$$U_s^*\left(\vec{x} - \frac{\vec{s}}{2}\right)U_s\left(\vec{x} + \frac{\vec{s}}{2}\right) = B(\vec{x}) \cdot \exp\left(\mathrm{i}\frac{k}{z}\vec{s} \cdot \vec{x}\right). \tag{9}$$

with the intensity envelop

$$B(\vec{x}) = \frac{1}{z^2}A\left(\vec{x} - \vec{s}/2\right)A\left(\vec{x} + \vec{s}/2\right) \tag{10}$$

and the second part of Eq. (9) being a linear phase ramp which depends both on the beam radius of curvature z and the shear $\vec{s}$. The ramp implies that the linear fringes of the interference pattern have a spatial carrier frequency of

$$\vec{\xi} = \frac{k\vec{s}}{2\pi z} = \frac{\vec{s}}{\lambda z}. \tag{11}$$

Equation (11) can be used in order to determine the shear s directly by taking the Fourier transform of the corresponding interference pattern. Hereafter, the shift Δ_ξ of the peaks across the Fourier domain is determined and thus the shear is

$$\vec{s} = \frac{\vec{\Delta}_\xi \lambda z}{N\Delta x}. \tag{12}$$

Here, N and Δx are the number of camera pixels in one direction and the pixel pitch, respectively.

3. EXPERIMENTAL RESULTS AND DISCUSSIONS

3.1 Experimental setup and the recorded interferograms

Figure 3 shows the experimental setup based on the scheme shown in Fig. 1. An impact ionization avalanche transit time (IMPATT) diode from TeraSense Corp. is used as a THz source which emits radiation at 280 GHz, ($\lambda = 1.07$ mm). A high gain diagonal horn serves to generate a Gaussian beam. A power of about 40 mW is directly measured behind the horn. The emitting spherical waves propagate through the RPG fabricated using mechanical milling on a block of high-density polyethylene (HDPE) with a computer numerical control (CNC) machine. The RPG is optimized for the 280 GHz beam.[30] The distance between the horn and the RPG is $z_1 = 150$ mm. A line-array THz camera consisting of 256 pixels with a pixel pitch of $\Delta x = 0.5$ mm is located at the output plane at $z_2 = 147$ mm from the RPG. To acquire two dimensional (2D) images, a scanning process along the horizontal axis using a PI translation stage was used.

Figure 4 shows examples of the recorded intensity patterns: The intensity profile of the test spherical wave field is shown in (a) and two interferograms resulting from the interference of the two shifted spherical wave fields

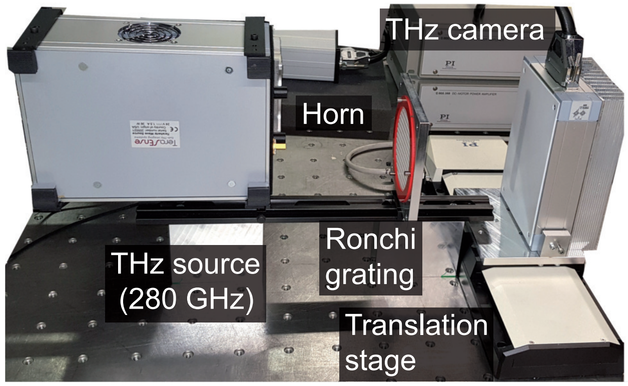

Figure 3. Photograph of the experimental shear interferometer setup. A continuous wave THz source emits a spherical wave at 280 GHz. A detachable high gain diagonal horn shapes the amplitude of the emitted spherical wave to a Gaussian envelope. The RPG, i.e the shear element, is inserted between the source and the line camera creating an overlap between the two copies of the test spherical wave. An intensity image of the wave field is recorded by moving the THz camera using a translation stage.

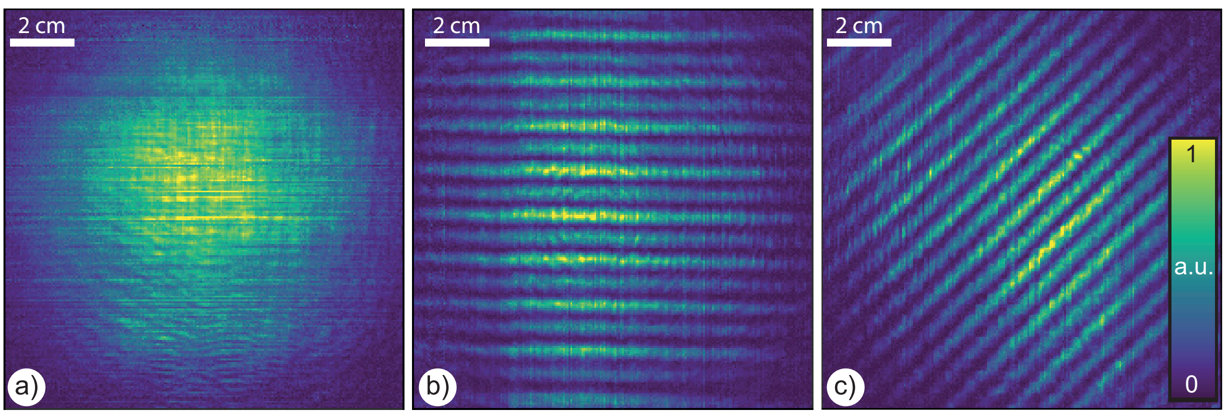

Figure 4. Captured intensity patterns: a) Intensity profile of the spherical wave captured at a distance of 297 mm from the source in the absence of RPG consistent with a Gaussian intensity envelope. b) and c) Two examples of the intensity interferograms captured after readjusting the RPG between the source and the camera for the shears $s_0 = [44, 0]$ mm and $s_4 = [30, 32.5]$ mm, respectively.

for two different shears are shown in (b) and (c), respectively. The recorded intensity profile of the investigated spherical wave field has a Gaussian profile. The two shears applied to capture the images shown in (b) and (c) are $s_0 = [44, 0]$ mm and $s_4 = [30, 32.5]$ mm obtained by rotating the RPG. As shown in Fig. 4, the interference patterns are composed of linear fringes generated in the overlap zone as theoretically expected from the coherent superposition of two shifted spherical wave fields.

Using the spatial carrier frequency method proposed to consider fringe rotation,[31] the phase difference $\Delta\phi = \phi_{+1} - \phi_{-1}$ is reconstructed from a single captured interferogram. Here, ϕ_{+1} and ϕ_{-1} are the spatial phase distributions of the spherical waves of the ± 1 diffraction orders. The results of the spatial phase shifting is shown in Fig. 5(a) for the s_4 shear measurements. For the wave front reconstruction the phase difference has to be unwrapped. The result of the unwrapping process using PUMA phase unwrapping technique[32] is shown in Fig. 5(b).

3.2 Wavefront reconstruction

In this section, we describe the method to reconstruct a wavefront from its measured finite differences $\Delta\phi$, which is an ill-posed inverse problem.[33] A solution for the problem is recently presented by minimizing the following

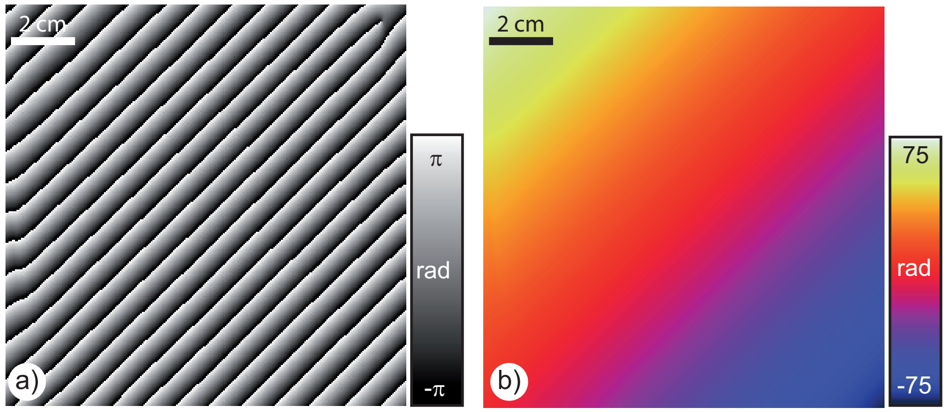

Figure 5. In a) an example of the phase difference reconstructed from the captured interferogram shown in Fig. 4(c) using the spatial carrier frequency approach, while in b) the corresponding phase unwrapped calculated using PUMA phase unwrapping technique.

objective function[34]

$$L(f) = \sum_{m=1}^{M} b(\vec{x}) \|\Delta_m f(\vec{x}) - \Delta_m \phi(\vec{x})\|^2 \,, \tag{13}$$

in order to find a wavefront estimate $\tilde{f}$ which minimizes L. In Eq. (13), $\| \cdots \|^2 = \sum_{\vec{x} \in R} | \cdots |^2$ and R refers to the grid of the camera and M represents the number of captured interferograms. Notice, that $b(\vec{x}) = \sqrt{B(\vec{x})}$ is a weighting factor which is defined in Eq. (10) and inherently obtained from the spatial carrier frequency method used to determine $\Delta\phi$ from the captured interference pattern. According to Eq. (13) the sum of the distance squared error (SDS-error) is minimized using the $M = 5$ shear measurements where the applied shears are $s_1 = [42, 12.5]$ mm, $s_2 = [37, 22.5]$ mm, $s_3 = [30, 32.5]$ mm, $s_4 = [22.5, 37]$ mm, and $s_5 = [12.5, 42]$ mm. A gradient-based iterative approach is used in the following to find the minimum of L which represents the least-squares solution of the reconstruction problem.[35] The approach is started with an initial guess $f^{(0)}$. At the l^{th} iteration, the current estimate $f^{(l)}$ maybe written in the form

$$f^{(l)} = f^{(l-1)} - \alpha^{(l-1)} \cdot \nabla L^{(l-1)} \,. \tag{14}$$

Such a scheme will be used to iteratively to improve the solution in the direction of the gradient ∇L with a scaling factor $\alpha^{(l-1)}$, which is defined for each iteration.[34] The iterative scheme stops if the SDS-error exhibits no further improvement, i.e., no changes in the consecutively recovered wavefront. The convergence solution of the minimisation is shown in Fig. 6(a), where the stop criteria was reached after 100 iterations.

To quantitatively evaluate the reconstructed wavefront, a Zernike polynomial decomposition was used.[36] This way, wavefront aberrations such as tilt and de-focus, could be accurately evaluated. In addition, the beam radius of curvature of the test spherical wave can be determined. The result of such an evaluation is shown in Fig. 6(b,c). In (b) we show the phase residuals obtained by subtracting the recovered wavefront from the ones reconstructed from the computed Zernike coefficients which are plotted in (c). From Fig. 6(b) we can estimate a standard deviation of $\sigma = 0.075$ mm which corresponds to approximately $\lambda/14$ root mean square wavefront error. In addition, one can see from Fig. 6(c) that the dominant mode is the 5^{th} one which corresponds to de-focus wavefront aberration, in other words, the wavefront exhibits only spherical aberration. The magnitude of the 5^{th} mode allows us to estimate the beam radius of curvature z which can be calculated from $z = r^2/4\mathcal{L}_5$,[36] where r is the aperture radius of the measurement. In our experiment, the values $D = 64$ mm and $\mathcal{L}_5 = 3.44$ mm give a beam radius of curvature of 297.67 mm which agrees very well with the geometrical model of the proposed experimental setup presented in Fig. 3.

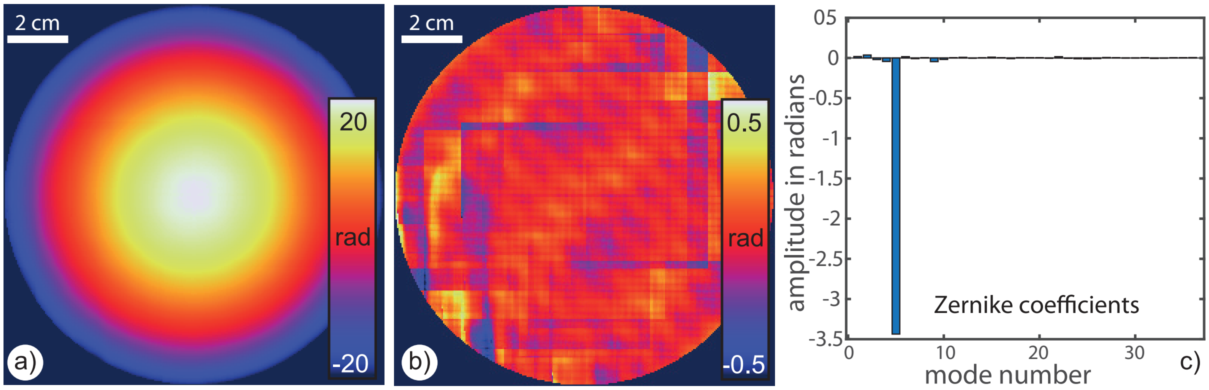

Figure 6. Experimental results: a) and b) Wavefront solutions of the iterative scheme for the test spherical wavefront and the residuals after fitting the recovered wavefront using Zernike polynomial decomposition. c) Computed Zernike coefficients of the first 36 Zernike polynomials.

4. CONCLUSIONS

We presented a simple THz common-path wavefront sensor based on a phase grating shear interferometer. The setup consists of a phase Ronchi grating located between the THz source and the camera. The phase grating is used as a shear element generating multiple copies of the test wavefront across the camera plane. We designed and fabricated a grating for optimal operation at 280 GHz. Based on the geometrical parameters of the setup such as the distances between the elements, the wavelength of the THz radiation and the parameters of the RPG (period and grooves depth) the setup is constructed so that the camera only captures the overlapped ± 1 diffraction orders. Across the overlap zone, the interference pattern is generated which is captured by the THz camera. The concept is verified by measuring a THz spherical wavefront from 5 shear experiments. These shear experiments where preformed varying the direction of the shear by rotating the RPG. Using the spatial carrier frequency method the phase difference was reconstructed from a single hologram. A gradient-based iterative process was used to recover the test spherical wavefront. We show, that the convergence of the process enables a wavefront reconstruction with a root mean square wavefront error of $\lambda/14$.

ACKNOWLEDGMENTS

This work is funded by the Deutsche Forschungsgemeinschaft (DFG) within the project ”SensATion” (project no. 423266368).

REFERENCES

[1] Tonouchi, M., “Cutting-edge terahertz technology,” *Nature photonics* **1**(2), 97–105 (2007).

[2] Lee, Y.-S., [*Principles of terahertz science and technology*], vol. 170, Springer Science & Business Media (2009).

[3] Taylor, Z. D., Singh, R. S., Bennett, D. B., Tewari, P., Kealey, C. P., Bajwa, N., Culjat, M. O., Stojadinovic, A., Lee, H., Hubschman, J.-P., et al., “THz medical imaging: in vivo hydration sensing,” *IEEE transactions on terahertz science and technology* **1**(1), 201–219 (2011).

[4] Soltani, A., Gebauer, D., Duschek, L., Fischer, B. M., Cölfen, H., and Koch, M., “Crystallization caught in the act with terahertz spectroscopy: Non-classical pathway for l-(+)-tartaric acid,” *Chemistry–A European Journal* **23**(57), 14128–14132 (2017).

[5] Kawase, K., Ogawa, Y., Watanabe, Y., and Inoue, H., “Non-destructive terahertz imaging of illicit drugs using spectral fingerprints,” *Optics Express* **11**(20), 2549–2554 (2003).

[6] Katletz, S., Pfleger, M., Pühringer, H., Mikulics, M., Vieweg, N., Peters, O., Scherger, B., Scheller, M., Koch, M., and Wiesauer, K., “Polarization sensitive terahertz imaging: detection of birefringence and optical axis,” *Optics Express* **20**(21), 23025–23035 (2012).

[7] Mittleman, D. M., "Twenty years of terahertz imaging," *Optics Express* **26**(8), 9417–9431 (2018).

[8] Jördens, C. and Koch, M., "Detection of foreign bodies in chocolate with pulsed terahertz spectroscopy," *Optical Engineering* **47**(3), 037003 (2008).

[9] Valzania, L., Zolliker, P., and Hack, E., "Topography of hidden objects using THz digital holography with multi-beam interferences," *Optics Express* **25**(10), 11038–11047 (2017).

[10] Afsah-Hejri, L., Hajeb, P., Ara, P., and Ehsani, R. J., "A comprehensive review on food applications of terahertz spectroscopy and imaging," *Comprehensive Reviews in Food Science and Food Safety* **18**(5), 1563–1621 (2019).

[11] Sun, Q., He, Y., Liu, K., Fan, S., Parrott, E. P. J., and Pickwell-MacPherson, E., "Recent advances in terahertz technology for biomedical applications," *Quantitative Imaging in Medicine and Surgery* **7**(3), 345 (2017).

[12] Rong, L., Latychevskaia, T., Chen, C., Wang, D., Yu, Z., Zhou, X., Li, Z., Huang, H., Wang, Y., and Zhou, Z., "Terahertz in-line digital holography of human hepatocellular carcinoma tissue," *Scientific Reports* **5**(1), 1–6 (2015).

[13] Hernandez-Cardoso, G. G., Amador-Medina, L. F., Gutierrez-Torres, G., Reyes-Reyes, E. S., Benavides Martínez, C. A., Cardona Espinoza, C., Arce Cruz, J., Salas-Gutierrez, I., Murillo-Ortíz, B. O., and Castro-Camus, E., "Terahertz imaging demonstrates its diagnostic potential and reveals a relationship between cutaneous dehydration and neuropathy for diabetic foot syndrome patients," *Scientific Reports* **13**, 3110 (2022).

[14] Boulogeorgos, A.-A. A., Alexiou, A., Merkle, T., Schubert, C., Elschner, R., Katsiotis, A., Stavrianos, P., Kritharidis, D., Chartsias, P.-K., Kokkoniemi, J., et al., "Terahertz technologies to deliver optical network quality of experience in wireless systems beyond 5g," *IEEE Communications Magazine* **56**(6), 144–151 (2018).

[15] Koch, M., "Terahertz communications: A 2020 vision," in [*Terahertz frequency detection and identification of materials and objects*], Miles, R. E., Zhang, X.-C., Eisele, H., and Krotkus, A., eds., 325–338, Springer (2007).

[16] Ghasempour, Y., Shrestha, R., Charous, A., Knightly, E., and Mittleman, D. M., "Single-shot link discovery for terahertz wireless networks," *Nature Communications* **11**(1), 1–6 (2020).

[17] Sengupta, K., Nagatsuma, T., and Mittleman, D. M., "Terahertz integrated electronic and hybrid electronic–photonic systems," *Nature Electronics* **1**(12), 622–635 (2018).

[18] Abdelghany, M., Farid, A. A., Rasekh, M. E., Madhow, U., and Rodwell, M. J., "A design framework for all-digital mmwave massive mimo with per-antenna nonlinearities," *IEEE Transactions on Wireless Communications* **20**(9), 5689–5701 (2021).

[19] Song, H.-J. and Nagatsuma, T., "Present and future of terahertz communications," *IEEE transactions on terahertz science and technology* **1**(1), 256–263 (2011).

[20] Yamagiwa, M., Minamikawa, T., Minamiji, F., Mizuno, T., Tokizane, Y., Oe, R., Koresawa, H., Mizutani, Y., Iwata, T., Yamamoto, H., et al., "Visualization of internal structure and internal stress in visibly opaque objects using full-field phase-shifting terahertz digital holography," *Optics Express* **27**(23), 33854–33868 (2019).

[21] Zhang, Y., Wang, C., Huai, B., Wang, S., Zhang, Y., Wang, D., Rong, L., and Zheng, Y., "Continuous-wave THz imaging for biomedical samples," *Applied Sciences* **11**(1), 71 (2021).

[22] Petrov, N. V., Perraud, J.-B., Chopard, A., Guillet, J.-P., Smolyanskaya, O. A., and Mounaix, P., "Terahertz phase retrieval imaging in reflection," *Optics Letters* **45**(15), 4168–4171 (2020).

[23] Valzania, L., Zolliker, P., and Hack, E., "Coherent reconstruction of a textile and a hidden object with terahertz radiation," *Optica* **6**(4), 518–523 (2019).

[24] Rong, L., Wang, S., Wang, D., Tan, F., Zhang, Y., Zhao, J., and Wang, Y., "Transport of intensity equation-based terahertz lensless full-field phase imaging," *Optics Letters* **46**(23), 5846–5849 (2021).

[25] Valzania, L., Feurer, T., Zolliker, P., and Hack, E., "Terahertz ptychography," *Optics Letters* **43**(3), 543–546 (2018).

[26] Hamza, A., Belal, A., Sokkar, T., El-Dessouky, H., and Agour, M., "Interferometric studies on the influence of temperature on the optical and dispersion parameters of grin optical fibre," *Optics and Lasers in Engineering* **45**(1), 145–152 (2007).

[27] Yassien, K. and Agour, M., "Digital holographic interferometry: optomechanical properties of fibers," *Polymer Engineering & Science* **51**(6), 1218–1225 (2011).

[28] Falldorf, C., Agour, M., Von Kopylow, C., and Bergmann, R. B., "Phase retrieval for optical inspection of technical components," *Journal of Optics* **14**(6), 065701 (2012).

[29] Falldorf, C., Agour, M., von Kopylow, C., and Bergmann, R. B., "Design of an optical system for phase retrieval based on a spatial light modulator," in [*AIP Conference Proceedings*], **1236**(1), 259–264, American Institute of Physics (2010).

[30] Agour, M., Falldorf, C., Taleb, F., Castro-Camus, E., Koch, M., and Bergmann, R. B., "Quasi-optical components for the THz-regime: Fabrication and characterization," *DGaO Proceedings* **122**, p9 (2021).

[31] Sokkar, T., El-Farahaty, K., El-Bakary, M., Omar, E., and Agour, M., "Characterization of axially tilted fibres utilizing a single-shot interference pattern," *Optics and Lasers in Engineering* **91**, 144–150 (2017).

[32] Bioucas-Dias, J. M. and Valadao, G., "Phase unwrapping via graph cuts," *IEEE Transactions on Image processing* **16**(3), 698–709 (2007).

[33] Servin, M., Cywiak, M., and Davila, A., "Lateral shearing interferometry: theoretical limits with practical consequences," *Optics Express* **15**(26), 17805–17818 (2007).

[34] Agour, M., Fallorf, C., Taleb, F., Castro-Camus, E., Koch, M., and Bergmann, R. B., "Terahertz referenceless wavefront sensing by means of computational shear-interferometry," *Optics Express* **30**, 7068–7081 (Feb 2022).

[35] Agour, M., Falldorf, C., and Bergmann, R. B., "Shape measurements of microscopic objects using computational shear interferometry," in [*Quantitative Phase Imaging II*], *Proc. SPIE* **9718**, 321–328, SPIE (2016).

[36] Binkele, T., Hilbig, D., Henning, T., and Fleischmann, F., "Determination of the paraxial focal length using zernike polynomials over different apertures," in [*Photonic Instrumentation Engineering IV*], *Proc. SPIE* **10110**, 60–69, SPIE (2017).